Postprint. Jiawei Ruan et al. Fuel, Volume 334 (2023) 126709
https://doi.org/10.1016/j.fuel.2022.126709

Experimental and theoretical study on efficient CO_2 absorption coordinated by molecules and ions of DBN and 1,2,4-triazole formed deep eutectic solvents

Jiawei Ruan [a], Xiangzhu Ye [a], Ruizhuan Wang [a], Lifang Chen [a,*], Liyuan Deng [b], Zhiwen Qi [a,*]

[a] *State Key Laboratory of Chemical Engineering, School of Chemical Engineering, East China University of Science and Technology, 130 Meilong Road, Shanghai 200237, China*

[b] *Department of Chemical Engineering, Norwegian University of Science and Technology (NTNU), Trondheim 7491, Norway*

[*] *Corresponding authors*: lchen@ecust.edu.cn (L. Chen); zwqi@ecust.edu.cn (Z. Qi)

Abstract: Deep eutectic solvents (DESs) as a novel class of designer solvents have attracted intensive attention in CO_2 capture, while the interactions between CO_2 and underlying molecules and/or ions in DESs are poorly understood. Here, superbase 1,5-diazabicyclo[4.3.0]non-5-ene (DBN) and 1,2,4-triazole (Tz) formed DESs with different DBN/Tz molar ratios were used to absorb CO_2, wherein DES [2DBN:Tz] achieved the highest weight capacity approaching 0.19 g CO_2/g DES at 25 °C. The ionicity of the DESs determined by hydrogen nuclear magnetic resonance (^{1}H NMR) showed a positive correlation with absorption capacity. Density functional theory calculation was also used to elucidate the proton transfer between molecular and ionic pairs in [DBN:Tz] and their interactions with CO_2. Both Hirshfeld atomic charge and electrostatic potential analyses revealed that DBN and Tz^- acted as electron-rich nucleophiles could form DBN-CO_2 and Tz-CO_2^- adducts with electrophilic CO_2, which were also confirmed by ^{13}C NMR and Fourier transform infrared spectroscopy. Moreover, a two-paths CO_2 capture process through synergistic effect of DBN and Tz^- was proposed and demonstrated.

Keywords: Deep eutectic solvents, superbase, ionicity, CO_2 capture, mechanism

1. Introduction

Carbon capture and storage (CCS) together with carbon capture and utilization (CCU) are considered as effective methods to alleviate the increasingly severe greenhouse effect, especially CO_2 emission from fossil fuels combustion [1,2]. As the first step in CCS and CCU technologies, efficient and reversible CO_2 capture has become one of the most attractive research hotspots [3,4]. Nitrogen chemisorption is widely used for CO_2 trapping, in which amine-based compounds serving as Lewis bases

can form N-C bond with weak acidic CO_2 [5,6]. Traditionally, aqueous solutions of amines have been used for industrial-level CO_2 removal [7,8]. However, the loss of volatile amines and the concurrent uptake of water into the gas stream could lead to substantial energy consumption and non-sustainable development [9].

Ionic liquids (ILs) as alternatives to aqueous amine solutions for CO_2 capture have drawn intensive attention due to their unique properties such as wide liquid range, flexible designability, negligible vapor pressure, and high thermal stability [10,11]. Combining the chemical reactivity of amines and ILs' superiorities, amine-based task-specific ILs are designed to overcome the main drawbacks of aqueous amines. Bates et al. firstly introduced amine-functionalized ILs for CO_2 capture, in which a primary amine moiety was tethered covalently to an imidazolium cation and exhibited increased CO_2 uptake approaching 0.5 mol CO_2/ mol IL at ambient conditions [12]. Subsequently, Wang et al. developed a series of azole-based ILs for equimolar CO_2 capture through strong Lewis basicity of the deprotonated azole anion [13].

Recently, mixtures of superbases and weak acids, referred to as protic ionic liquids (PILs), have shown excellent performance for CO_2 absorption owing to their strong affinity with CO_2 and low viscosity [14,15]. Generally, these mixtures were prepared by the neutralization of strong proton acceptors such as 1,8-diazabicyclo[5.4.0]undec-7-ene (DBU), 1,5-diazabicyclo[4.3.0]non-5-ene (DBN), 1,1,3,3-tetramethylguanidine, and 1,3,4,6,7,8-hexahydro-1-methyl-2H-pyrimido[1,2-a]pyrimidine with weak proton donors including pyrrole, imidazole, 1,2,4-triazole (Tz), benzimidazole, phenol, ethylene glycol, etc. The pioneering work was switchable solvents composed of DBU and an alcohol that can reversibly capture CO_2 [16]. A series of functionalized choline-based ILs were prepared and exhibited considerable CO_2 capture capacity up to 28.6 wt%, which was attributed to the formation of carbonic acids together with carbamates [17]. To obtain higher absorption capacity, superbase was added to increase the number of active sites in the absorption system [18]. Furthermore, Zhang et al. found the protonated superbase cation played a key role in absorption and manifested a synergistic CO_2 capture mechanism through cation and anion effects [19]. Most studies have revealed the absorption mechanism, which involved the formation of carbonates and/or carbamates by nucleophilic attacks of deprotonated basic anions on CO_2 [20].

It is worth noting that mixtures of bases and weak proton acids are not only composed of ions but also molecular species due to the restriction of proton transfer equilibrium [21], leading to the presence of complex hydrogen bond networks among

ionic and molecular species. Different from ILs composed of ions, deep eutectic solvents (DESs), defined by Smith and Abbott et al., are systems formed from a eutectic mixture of Lewis or Brønsted acids as hydrogen bond donors (HBDs) and bases as hydrogen bond acceptors (HBAs) that can contain a variety of ionic and molecular species [22]. In this regard, the mixture of superbase and weak proton acid seems to be more suitable referred to DESs if hydrogen bond interaction is prominent. Moreover, the ionicity of DESs should be considered because molecular and ionic states are dependent mutually and will jointly determine the performance of DESs.

Spectral and theoretical calculation methods have been used to investigate the ionicity and degree of proton transfer in acetate-based PILs, unravelling the effect of base structure, p*K*a, and hydrogen bond network [23-25]. Lately, a quantitative ionicity determination method was established by assuming the active hydrogen chemical shift to be a weighted average of that can be observed in acid and protonated base [26]. In this way, a new cooperative CO_2 absorption mechanism by both HBD and deprotonated HBD anion was proposed through absorptive capacity combined with ionicity calculation in DBU-based DESs [27]. Elucidating the coexistence of molecules and ions in DESs and their diverse interactions with CO_2 are of great significance in the CO_2 trapping process. Although a few studies have shown various CO_2 capture mechanisms in which superbase can protonate the HBD and stabilize the absorption products of anion and CO_2 [18,19,27], the insight into the direct CO_2 absorption by superbase molecules and ions in DESs has scarcely been reported.

Herein, we synthesized a type of DESs by superbase DBN and weak acid Tz for CO_2 capture. The degree of proton transfer in the DESs was determined and the proton transfer process from Tz to DBN was testified. The interactions in molecular complexes and ionic pairs together with their independent interactions with CO_2 were also analyzed. In addition, the direct absorption of CO_2 by DBN molecules and Tz^- ions was confirmed by the relationship between absorption capacity and ionicity of the DESs together with spectroscopy. A two-paths CO_2 capture process was also proposed.

2. Materials and methods

2.1. Materials

Tz (99%) and DBN (98%) were purchased from Shanghai Macklin Biochemical Co., Ltd., China. CO_2 with a mole fraction of 0.9999 was supplied by the Shanghai Wetry Standard Reference Gas Co., Ltd., China. The nuclear magnetic resonance (NMR)

solvents, deuterated dimethyl sulfoxide (99.9% DMSO-d_6, 0.03 vol% tetramethylsilane, TMS) and deuterated acetonitrile (99.8% CD_3CN, 0.03 vol% TMS), were obtained from Cambridge Isotope Laboratories, Inc., USA and Shanghai Macklin Biochemical Co., Ltd., China, respectively. All chemicals were directly used without further purification. In particular, anhydrous DBN used for direct CO_2 absorption was treated under vacuum drying by a rotary evaporator at 60 °C for 8 h and then dried using 3A molecular sieves to eliminate the influence of water on absorption.

2.2. DES preparation and characterization

DESs were prepared by mixed DBN and Tz with a certain molar ratio from 3:1 to 1:3 denoted as [3DBN:Tz], [2DBN:Tz], [DBN:Tz], [DBN:2Tz], and [DBN:3Tz]. Typically, appropriate amounts of DBN and Tz were weighted with a precision of 0.0001 g. Then the mixture was added to a dried flask under nitrogen protection and stirred at 40 °C for 6 h to ensure thorough homogeneity. Afterwards, the prepared DES was dried at 60 °C through rotary evaporation under vacuum for at least 8 h to ensure the water content less than 0.2 wt%. The water content of the DESs was measured by AQV-300 Karl-Fisher volumetric titration (Hiranuma, Japan).

The prepared DESs were characterized by ^{1}H NMR and Fourier transform infrared spectroscopy (FT-IR). ^{1}H NMR and ^{13}C NMR spectra were measured on a 600 MHz spectrometer (Ascend 600, Bruker, Germany) with 128 scans in DMSO-d_6 and 1024 scans in CD_3CN at 25 °C, respectively, and all spectra were referenced to TMS. Before ^{1}H NMR measurement, 30 mg prepared DES sample was injected into a 5 mm NMR tube together with 0.6 mL DMSO-d_6. Notably, the mass concentration of all ^{1}H NMR samples were controlled as equal as possible. FT-IR spectra were obtained by Nicolet iS20 spectrometer (Thermo Scientific, USA) operating in the attenuated total reflection (ATR) mode.

The melting points of DESs were determined by differential scanning calorimetry (DSC, TA Instruments DSC 25, USA). DESs were loaded into TA Tzero aluminum pans in glove box under N_2. The sample was firstly cooled to -90 °C at a rate of 0.1 °C/min to ensure complete crystallization. After isothermal for 2 h, the sample was heated to 50 °C at a rate of 10 °C/min and the melting point was taken from the onset temperature of the endothermic peak appearing in the heating process.

2.3. CO_2 absorption and desorption procedure

CO_2 capture was performed in an apparatus reported by our previous works, as

illustrated in Fig. S1 (Supporting Information) [28,29]. A pressure transmitter (Series 33X, Keller Co., Switzerland) with an accuracy of ± 0.2 kPa was set up between the storage tank (V_s = 150 ± 0.1 mL) and the stainless-steel autoclave (V_r = 30 ± 0.1 mL) to measure the pressure at intervals of 0.1 s. Typically, after 1 g of DESs was added into the autoclave, the system was evacuated with a vacuum pump to a pressure lower than 3 kPa and then set at a certain temperature, pressure, and stirring speed. The CO_2 capture reached an absorption equilibrium when the pressure remained constant. The CO_2 absorption capacity was determined by a differential pressure method [30]. For the desorption process, the autoclave was heated and kept at 80 °C with vigorous stirring, and the pressure was also recorded in real-time until constant atmospheric pressure.

2.4. Computational details

Theoretical calculations were conducted using Gaussian 09 E.01 software package. The geometric configurations were optimized at the B3LYP/6-311+G(d,p) level with DFT-D3(BJ) empirical dispersion correction. The calculation was performed in a continuum solvation model based on the quantum mechanical charge density (SMD solvation model) [31]. DBN, with a dielectric constant of 3.06 estimated by the Clausius-Mossotti equation [32], was used as the solvent to simulate the environment of DBN-Tz DESs. Further frequency calculation at the same level of theory was also performed at the optimized geometries to ensure no imaginary frequency. The counterpoise (CP) technique was employed to correct the basis set superposition error (BSSE) problem for calculating the interaction energy (ΔE_{BSSE}). The enthalpy changes of each optimized geometry were obtained via vibrational frequency analysis at 25 °C and 100 kPa. Furthermore, the intrinsic reaction coordinate (IRC) pathways were traced to verify the energy profile connecting the transition state (TS) to the two minima of the proton transfer reaction. Atom in molecules (AIM) analyses were performed to confirm the existence and characteristics of the hydrogen bond network between molecule complexes and ionic pairs. Hirshfeld atomic charges and electrostatic potential (ESP) analyses were conducted to search for the potential nucleophilic and electrophilic sites between DESs and CO_2. AIM, ESP, and Hirshfeld atomic charge analyses were all performed based on the B3LYP-D3(BJ)/6-311+G(d,p) wave function using the Multiwfn version 3.8 code [33].

3. Results and discussion

3.1. DES performance

DSC curves and corresponding fusing points of DBN and Tz mixtures investigated in this work are shown in Fig. 1, indicating these DESs are liquids at room temperature and can be directly used to capture CO_2. Since the definition of DESs is that the melting point at the eutectic composition is much lower than that of a theoretical ideal mixture, the experimental melting points together with the liquidus line (grey dot dash line) of ideal mixture of DBN and Tz are exhibited in Fig. S2, which is calculated based on the melting temperature and fusion enthalpy of pure DBN (-39.5 °C and 5.87 kJ/mol) and Tz (120 °C and 14.5 kJ/mol) measured in this work. Compared to hypothetical ideal mixture, the mixtures formed by DBN and Tz show significant melting point depression, which indicates the strong hydrogen bond interaction and the formation of DESs [34,35]. As for the measured melting points of DESs investigated in this work, they are depicted in Fig. 1 and Fig. S2. With increased amount of DBN from [DBN:2Tz] to [3DBN:TZ], the melting points of the DESs decrease from -56.6 °C to -89.7 °C. The DESs are difficult to crystallize with further increasing amount of DBN, and the potential deep eutectic point is incapable to measure. In addition, we previously found DESs formed by weak base and strong acid have shown two eutectic points in full solid-liquid phase diagram, which is ascribed to the formation of high melting point equimolar salts and the change of hydrogen bond acceptor and donor with tuning molar ratio of HBA and HBD [36]. Thus, the lower melting temperature of [DBN:3Tz] than that of [DBN:2Tz] may be attributed to formation of high melting point salts at X_{Tz} close to 0.6 (Fig. S2). Furthermore, according to the independent gradient model based on Hirshfeld partition (IGMH) analysis [37] in Fig. S3, optimized geometric configurations of [DBN:3Tz] exhibits increased hydrogen bonding sites but decreased interaction strength compared to [DBN:Tz] and [DBN:2Tz], which may synergistically account for the decreased melting point of [DBN:3Tz].

Postprint. Jiawei Ruan et al. Fuel, Volume 334 (2023) 126709
https://doi.org/10.1016/j.fuel.2022.126709

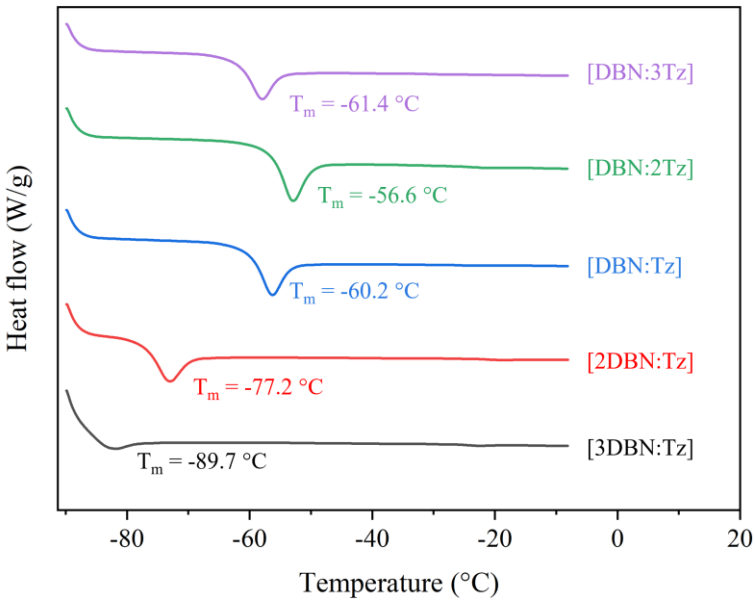

Fig. 1. DSC curves and corresponding melting points of DBN-Tz DESs.

The ionicity of the DESs was calculated by the NMR technique according to the previously reported method [26,38]. Herein, a brief introduction is provided to clarify the calculation process in DBN-Tz DESs.

The proton transfer equilibrium in DBN-Tz DESs can be described as follows:

	DBN	+	Tz	⇔	$DBNH^+$	+	Tz^-
I	X_{DBN}		X_{Tz}		0		0
C	X_{DBNH}		X_{DBNH}		X_{DBNH}		X_{DBNH}
E	X_{DBN} - X_{DBNH}		X_{Tz} - X_{DBNH}		X_{DBNH}		X_{DBNH}

where I is the initial concentration, C is the change of concentration, and E is the equilibrium concentration.

The equilibrium constant K_{eq} can be expressed as Eq. (1):

$$K_{eq} = \frac{X_{DBNH}^2}{(X_{DBN}-X_{DBNH})(X_{Tz}-X_{DBNH})} \quad (1)$$

According to Shen et al. [26], the observed ^{1}H NMR chemical shift was assumed to be the weighted average of the unreacted molecule Tz and protonated ion $DBNH^+$. As only one type of exchangeable proton involves in DBN-Tz DESs, the observed chemical shift δ can be described as Eq. (2):

$$\delta = \delta_{Tz} \times (X_{Tz} - X_{DBNH}) + \delta_{DBNH} \times X_{DBNH} \quad (2)$$

where δ is the observed chemical shift of active hydrogen in DES (Fig. 2a), δ_{Tz} and δ_{DBNH} are the chemical shift of active hydrogen in Tz and $DBNH^+$, respectively.

A series of samples with different molar ratios of DBN to Tz were synthesized and their chemical shifts of exchangeable protons from ^{1}H NMR spectra were used to

calculate the contents of molecular and ionic components, as shown in Fig. 2. With the increased amount of DBN, the active hydrogen peak gradually shifts to downfield, which results from enhanced hydrogen bond interaction between DBN with Tz. Meanwhile, the peaks become broad, indicating the active protons are in different equilibrium states between molecular and ionic species [39]. Thus, the observed chemical shift δ is taken from the corresponding maximum peak (Fig. 2a and Fig. S4). Hence, each mixture can give Eqs (1) and (2), and the least-squares method is applied to fit the experimental data. The active proton from Tz, δ_{Tz}, should be different in pure substrate or DESs [38], and δ_{Tz} together with δ_{DBNH} and K_{eq} are regarded as parameters in fitting process. With a certain optimization, three unknown constants could be calculated. The correlation coefficient is 0.996 and root mean square error is 0.038, which fit well with the experimental data (Fig. 2b). The calculated results are as follows: K_{eq} = 5.05, δ_{DBNH} = 9.72, δ_{Tz} = 8.589.

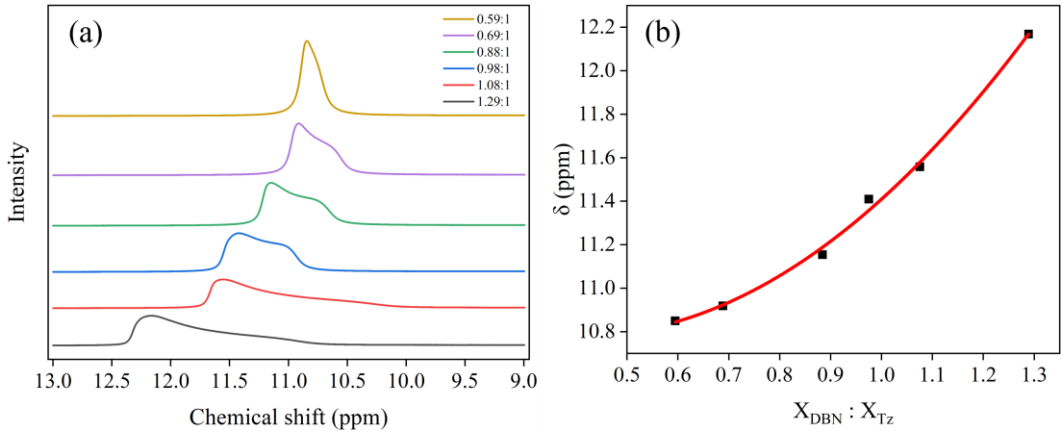

Fig. 2. (a) Chemical shifts from ^{1}H NMR and (b) optimization results of active hydrogen in DBN-Tz DESs with various molar ratios of DBN to Tz.

X_{DBNH} and ionicity of DESs with different molar ratios of DBN to Tz, can be calculated according to Eq. (1). The calculated ionicity values of DESs with a molar ratio of DBN/Tz from 3:1 to 1:1 are 92%, 87%, and 69%, respectively. Significantly, the ionicity of the DESs under various DBN/Tz molar ratios is not equal to the proportion of ions in the DESs system but represents the extent of proton transfer which equals to the conversion of the component at a relatively low initial concentration. The ionicity shows a positive correlation with the DBN/Tz ratio, which can be ascribed to the fact that an increased DBN amount can shift the proton transfer equilibrium forward. Notably, the ionicity of [DBN:Tz] is 69%, indicating the coexistence of molecules and ions in the DES.

Postprint. Jiawei Ruan et al. Fuel, Volume 334 (2023) 126709
https://doi.org/10.1016/j.fuel.2022.126709

3.2. Molecular complexes and ionic pairs in DESs

Based on the ionicity calculation, the proton transfer from molecular complex to ionic pair together with the interactions between them is also revealed at a molecular level by DFT calculation using DES [DBN:Tz] as an example. For the proton transfer process in [DBN:Tz], IRC pathways were traced to verify the energy profile connecting TS to optimized molecular complex and ionic pair configuration. As energy profile shown in Fig. 3, the proton transfer reaction is endothermic, and the energy barrier is 14.1 kJ/mol which is close to that of proton transfer between bis-(2-methoxyethyl)-ammonium and acetate reported previously [40]. Such a low energy barrier also indicates the rapid kinetics and reversibility of the proton transfer reaction. Thus, the proton transfer can quickly achieve equilibrium under a controlled preparation temperature at only 40 °C. Initially, the N-H bond length of Tz in DBN-Tz molecule pair (mol-pair) is 1.06 Å. Then, the proton will transfer from Tz to DBN and form $DBNH^+$ in which the new N-H bond length is 1.08 Å.

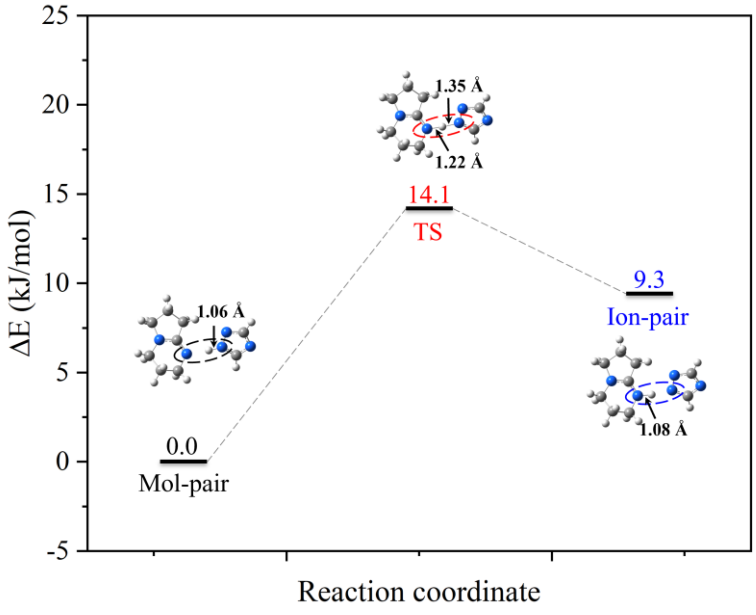

Fig. 3. Energy profile of proton transfer between mol-pair and ion-pair in [DBN:Tz].

The mol-pair undergoes a TS in which DBN and Tz compete for the proton, resulting in the formation of ionic pair (ion-pair) with complex hydrogen bond networks. Topological analyses based on AIM theory were performed to further locate and clarify the characteristic of weak interactions in mol-pair and ion-pair. The visualized AIM results were obtained by finding chemical bond critical points (BCPs) and topological paths (Fig. S5). The serial numbers of BCPs and labels of involved atoms are also shown in the figure. The orange ball and line illustrate the BCPs and topological paths

connecting atoms, which means weak interactions. In addition, the topological parameters at the BCPs including electron density (ρ_{BCP}), Laplacian values of electron density ($\nabla^2\rho$), and energy density ($E_{(r)}$) together with interaction energy with the BSSE correction (ΔE_{BSSE}) are listed in Table 1.

Table 1 Calculated binding energy (ΔE_{BSSE}, kJ/mol) and topological parameters (ρ_{BCP}, $\nabla^2\rho$, $E_{(r)}$, a.u.) at the BCPs for weak interactions in mol-pair and ion-pair.

type	BCP	ρ_{BCP}	$\nabla^2\rho$	$E_{(r)}$	ΔE_{BSSE}
Mol-pair	1	0.0568	0.0974	-0.0137	-51.9
	2	0.0058	0.0166	0.0006	
Ion-pair	3	0.0682	0.0929	-0.0215	-148.7
	4	0.0109	0.0314	0.0012	

As shown in Fig. S5 and Table 1, there are two types of BCPs in both mol-pairs and ion-pairs, which can be expressed N-H···N (BCP 1 in mol-pair, BCP 3 in ion-pair) and C-H···N (BCP 2 in mol-pair, BCP 4 in ion-pair). According to the topological analyses in the AIM theory, ρ_{BCP} is positively correlated with the bond strength [41], and the type of bond is characterized by $\nabla^2\rho$ and $E_{(r)}$, for which positive $\nabla^2\rho$ values usually refer to non-covalent bonds including ionic bonds, hydrogen bonds, and van der Waals interactions. Based on the topological parameters in mol-pair and ion-pair, the interaction of N-H···N type in the DES [DBN:Tz] is typical hydrogen bond [42]. Considering relatively small ρ_{BCP} and $\nabla^2\rho$ values together with positive $E_{(r)}$ value, the C-H···N type belongs to van der Waal interactions. In addition, the interaction energies of ion-pairs are larger than that of mol-pairs, owing to the stronger Coulomb force in ion-pairs.

The topological analyses reveal the complex hydrogen bond networks in DES [DBN:Tz] including neutral hydrogen bonds between neutral DBN-Tz complexes and doubly ionic hydrogen bonds between ionic $DBNH^+$-Tz^- pairs. Hydrogen bond interactions which originate from the competition for exchangeable proton between DBN and Tz can be the driving force of proton transfer and may further determine the equilibrium of the molecular complexes and ionic pairs. Therefore, the stronger hydrogen bond interaction in ion-pair is in good agreement with the calculated ionicity of 69% which suggests the more abundant ionic species in the DES [DBN:Tz].

3.3. CO_2 absorption

The CO_2 absorption performance of DBN-Tz DESs with different ionicities was measured to determine the optimal absorption temperature and DBN/Tz molar ratio,

along with the relationship between ionicity and absorption capacity. Fig. 4 shows the molar absorption capacity by DBN-Tz DESs (1 mol DES contains 1:n or n:1 mol HBA/HBD, n = 1, 2, and 3) at different molar ratios and temperatures. Overall, the CO_2 absorption capacity increases with the increased molar ratio of DBN to Tz. The maximum absorption capacity of [3DBN:Tz] reaches 1.89 mol CO_2/mol DES at 25 °C. The absorption temperature also greatly influences the maximum absorption capacity. The molar CO_2 absorption capacity of DESs with DBN/Tz molar ratio from 3:1 to 1:2 at 25 °C is larger than those at 35 and 45 °C, indicating that CO_2 absorption is an exothermic process. As for [DBN:3Tz], the temperature shows a positive effect on CO_2 absorption, which means the mass transfer is strictly limited at low temperature due to its high viscosity.

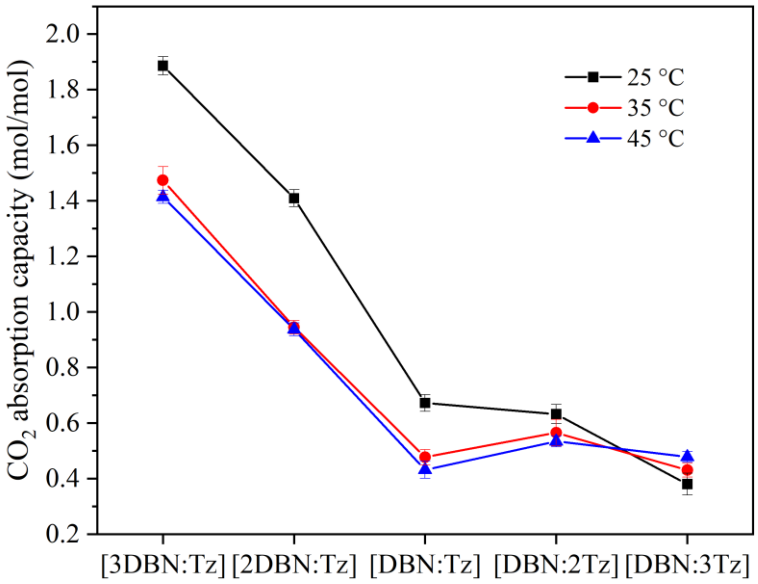

Fig. 4. Molar absorption capacity of CO_2 by DBN-Tz DESs at different temperatures.

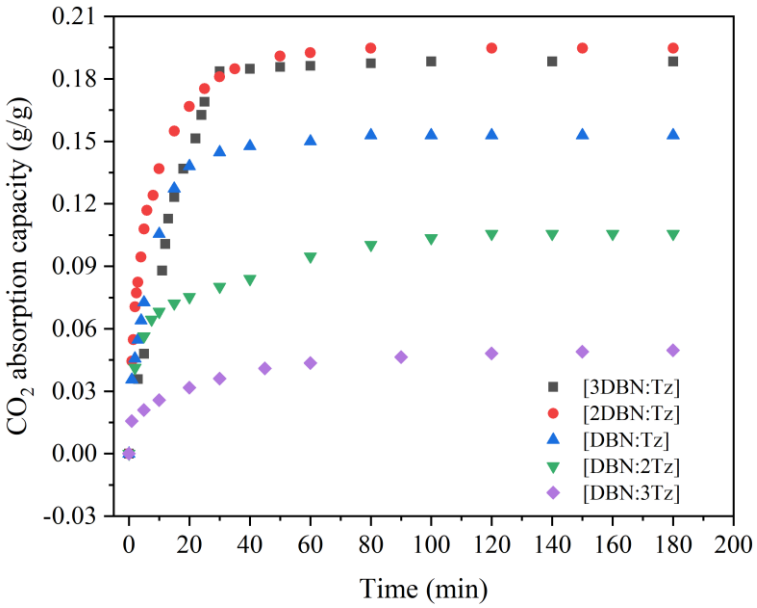

Fig. 5. CO_2 gravimetric absorption capacity by DBN-Tz DESs under different molar ratios at 25 °C and 100 kPa.

For the CO_2 capacity of DESs, the weight absorption capacity is more practical for industrial absorbent evaluation, while the molar absorption capacity can be used for further mechanism analysis. As time-dependent CO_2 gravimetric absorption capacity illustrated in Fig. 5, the absorption rate increases as the DBN ratio increases. [3DBN:Tz] firstly reaches absorption equilibrium after 30 min, while [DBN:3Tz] takes 180 min. Nonetheless, [2DBN:Tz] obtains the highest weight capacity approaching 0.19 g CO_2/g DES in 60 min.

For the molar absorption capacity, we found that the molar CO_2 uptake of both [2DBN:Tz] and [3DBN:Tz] exceed 1 mol per mol DES. It is speculated that there are species other than Tz^- in DBN-Tz DESs can capture a considerable amount of CO_2, because the deprotonated Tz^- can only absorb equimolar CO_2 through N-C bond formation [13,17]. Moreover, the molar capacity of DESs increases with the increase of the DBN/Tz ratio, which suggests the superbase DBN can facilitate CO_2 absorption.

To check the possibility of direct CO_2 absorption by DBN, the absorption capacity of anhydrous DBN was also measured. Water content in anhydrous DBN was less than 0.04% in order to prevent the formation of bicarbonate to the greatest extent during absorption. The results show that 1 mol DBN can absorb 0.5 mol CO_2, which seems like that DBN can react with CO_2 in a stoichiometric of 2:1. However, according to earlier work [43], the measured conversion of DBN and CO_2 was 60% at -10 to 0 °C for 2 h, wherein the DBN can bind with equimolar CO_2 and for DBN-CO_2 adduct. Taking into consideration the CO_2 process is exothermic, the chemical equilibrium of

absorption will shift inversely when absorption temperature increases. Thus, the measured absorption capacity of 0.5 mol CO_2/mol DBN means that the yield of binding reaction of DBN and CO_2 is 50% under experimental condition.

The CO_2 capture by Tz^- follows a 1:1 absorption mechanism [44] and the absorption ratio of DBN molecule to CO_2 can be tentatively regarded as 2:1. If no species other than DBN and Tz^- are directly involved in the absorption, the ideal CO_2 uptake capacity of DBN-Tz DESs, C_{ideal}, can be deduced and expressed as Eq. (3):

$$C_{ideal} = I + (X_{DBN} - I) \times 50\% \quad (3)$$

where X_{DBN} is the initial molar ratio of DBN to Tz (X_{DBN} = 1, 2, and 3) and I is the ionicity of the corresponding DES. The measured and ideal CO_2 absorption molar capacities and previously determined ionicity are shown in Table 2. It is reasonable that the actual measured CO_2 capacity is lower than the ideal capacity due to viscosity limitation. The deviation between measured and ideal capacities seems to decrease as the DBN molar ratio increases, indicating the influence of mass transfer resistance on the reaction equilibrium reduces with increased DBN/Tz molar ratio. The molar absorption capacities of [2DBN:Tz] and [3DBN:Tz] are 1.41 and 1.89, respectively, which is very close to the corresponding ideal capacities. Thus, the relationship among measured CO_2 uptake, ideal CO_2 uptake, and ionicity gives a basic understanding of the plausible absorption processes in which both DBN molecules and Tz^- ions can directly absorb CO_2.

Table 2 Measured (25 °C, 100 kPa) and ideal CO_2 absorption molar uptake and calculated ionicity (25 °C) of DES under different molar ratios.

sample	Measured uptake (mol CO_2/mol system)	Ideal uptake (mol CO_2/mol system)	Calculated ionicity
Anhydrous DBN	0.50	-	-
[3DBN:Tz]	1.89	1.96	0.92
[2DBN:Tz]	1.41	1.44	0.87
[DBN:Tz]	0.67	0.85	0.69
[DBN:2Tz]	0.63	0.94	0.87
[DBN:3Tz]	0.38	0.96	0.92

3.4. Mechanism of CO_2 absorption

To uncover the CO_2 absorption mechanism by DBN-Tz DESs, theoretical calculation was employed to elucidate the multiple interactions between CO_2 and DESs

which contain molecules and ions in it. Herein, Hirshfeld atomic charges of nitrogen, carbon, and oxygen atoms in DBN, $DBNH^+$, Tz, and Tz^- together with CO_2 are calculated and shown in Fig. 6. Corresponding ESP isosurface maps of complexes including molecule or ion with CO_2 are shown inset. It has been widely accepted that an atom with a more positive (negative) atomic charge is more likely to be the preferential site of nucleophilic (electrophilic) reaction [45]. As can be seen in Fig. 6, the C atom in CO_2 exhibits a large positive atomic charge (0.3408 a.u.), indicating CO_2 is vulnerable to nucleophilic attack. Taking into consideration of N(2) atom in DBN-based species, DBN and $DBNH^+$, the N(2) atom in DBN (Fig. 6a) shows a significant negative atomic charge (-0.1785 a.u.), while the atomic charge of N(2) atom in $DBNH^+$ (Fig. 6b) increases to -0.0623 a.u.. Thus, as an electron-rich nucleophile, DBN can attack C atom in CO_2, while $DBNH^+$ seems to be unable to react with inert CO_2. This result is also in accordance with the corresponding ESP maps in which the N(2) atom in DBN can attract the C atom of CO_2, while C(5) atom shows greater affinity to CO_2 than N(2) atom in $DBNH^+$.

As for Tz and Tz^-, the Hirshfeld atomic charge of N(1) atom attached to the active hydrogen in Tz is -0.0161 a.u.. After deprotonation, the atomic charge of N(1) atom in Tz^- significantly decreases to -0.2273 a.u. because of the π-electron delocalization in Tz^- ring, thereby leading to enhanced interaction between N(1) atom in the Tz^- and CO_2. Moreover, the nitrogen atom in neutral pyridine has poor ability for CO_2 capture and only form weak van der Waals complexes with CO_2 [46,47]. Thus, as another structurally related nitrogen-containing heterocyclic compound, Tz molecule is also difficult to bind CO_2. In short, both Hirshfeld atomic charge and ESP analyses demonstrate that DBN molecule and Tz^- ion can form nucleophilic interaction on the electrophilic C atom in CO_2 in DBN-Tz DESs. DBN and Tz^- are firstly pulled to the reaction site in CO_2 through electrostatic attraction and new bonds are then formed through electron transfer.

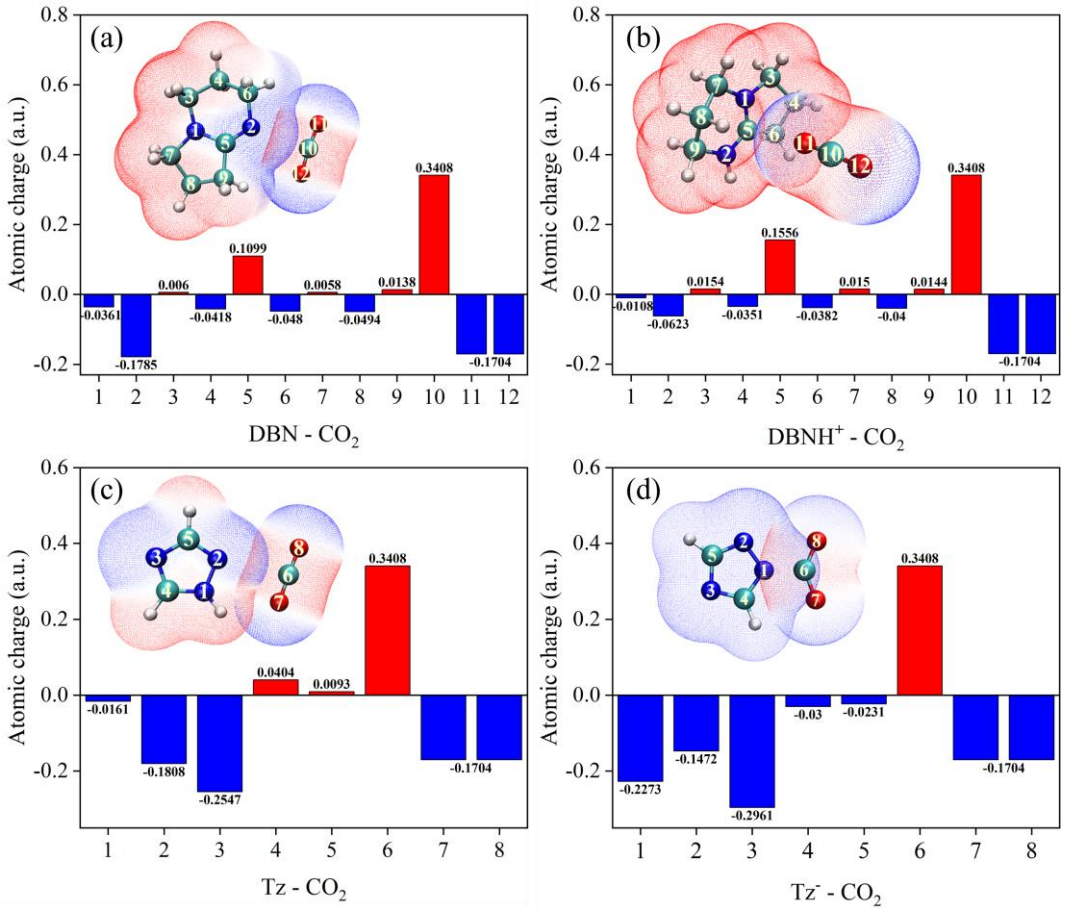

Fig. 6. Hirshfeld atomic charge and ESP isosurface map (inset) between CO_2 and (a) DBN, (b) $DBNH^+$, (c) Tz, and (d) Tz^- in DBN-Tz DESs. Red color represents the positive atomic charge and electrostatic potential, while blue color represents the negative atomic charge and electrostatic potential. The numbers on the X-axis correspond to the atoms (Blue N atom, Red O atom, Green C atom) in the ESP map.

The multiple interactions of DBN and Tz^- in DBN-Tz DESs with CO_2 were further investigated by ^{13}C NMR and FT-IR to support the experimental and theoretical results. Anhydrous DBN can form DBN-CO_2 adducts, while the products become bicarbonates in the presence of water [48]. To confirm the formation of DBN-CO_2 instead of bicarbonates, we measured the CO_2 absorption capacity of anhydrous DBN and a mixture of DBN and equimolar deionized water. The results are in line with our expectation and the CO_2 absorption capacities for anhydrous DBN and hydrous DBN are 0.50 and 0.95 mol CO_2/mol absorbent, respectively, since CO_2 capture by deprotonated H_2O obeys the 1:1 absorption process.

The ^{13}C NMR spectra of anhydrous DBN together with absorption products of anhydrous DBN and hydrous DBN are shown in Fig. 7. The amidine (-N=C-N-) carbon in anhydrous DBN appears at 161.2 ppm, as shown in Fig. 7a. The products of

anhydrous DBN after CO_2 absorption (Fig. 7b) shows two low-intensity signals at 160.3 and 163.0 ppm (weaker) assigned to a carbamate (-N-COO) and an amidine (-N=C-N-) carbon, respectively [43]. The peak of amidine (-N=C-N-) carbon at 161.2 ppm moves downfield to 163.0 ppm during the CO_2 absorption by DBN. It is attributed to the newly formed N-C bond, which reduces the electron density of the amidine atom adjacent to the N(2) atom of DBN.

Fig. 7c also shows two low-intensity signals at 159.6 and 164.0 ppm with similar intensities assigned to an amidine (-N=C-N-) carbon and bicarbonate ion (HCO_3^-). For bicarbonate, the peak of amidine carbon moves upfield to 159.6 ppm due to the electric field effect [49]. DBN generates a local electric field after protonation to $DBNH^+$, which causes the polarization of the adjacent amidine bond and increases the electron density of amidine carbon, and then the chemical shift of amidine carbon shifts to upfield. In addition, considering the peak shape of amidine carbon in Fig. 7a (161.2 ppm) and Fig. 7c (159.6 ppm) with split peaks including one tiny and another high intensity, the peak at 159.6 ppm should also be assigned to corresponding amidine carbon in $DBNH^+$. Accordingly, the peak at 160.3 ppm in Fig.7b and the peak at 164.0 ppm in Fig. 7c can be recognized as different species, assigned to (-N-COO) in DBN-CO_2 adduct and (HCO_3^-) in bicarbonate, respectively [50,51].

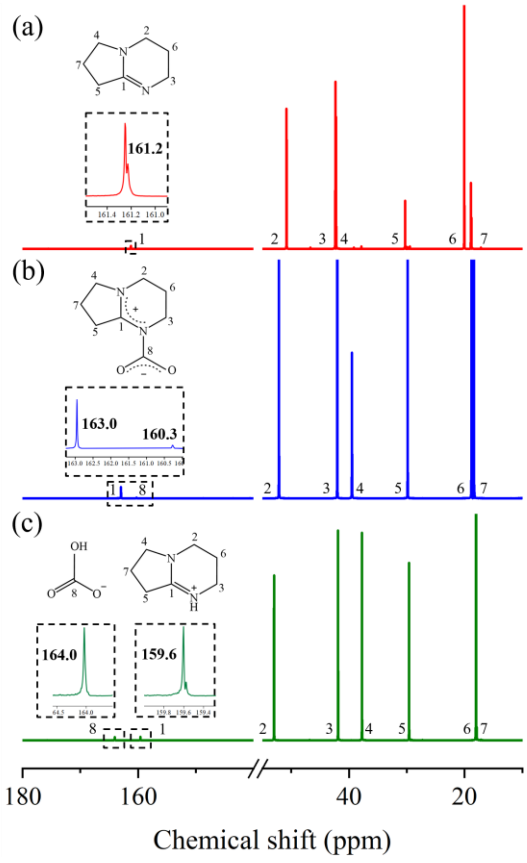

Fig. 7. ^{13}C spectra of (a) anhydrous DBN, (b) products of DBN + CO_2 under anhydrous condition, (c) products of DBN diluted in equimolar deionized water + CO_2. The insets are DBN, proposed DBN-CO_2 adduct, and bicarbonate structures consistent with observed spectra.

Based on ionicity calculation and CO_2 absorption capacity measurement, containing abundant DBN molecules and Tz^- ions, DES [2DBN:Tz] possesses the highest gravimetric absorption capacity at 25 °C. Thus, ^{13}C NMR and FT-IR spectra of [2DBN:Tz] before and after CO_2 treatment are exhibited in Fig. 8 to further manifest the synergistic absorption mechanism. The ^{13}C NMR of the CO_2 saturated [2DBN:Tz] has two new peaks at 160.0 and 163.2 ppm. The peak at 160.0 ppm close to the (-N-COO) peak in DBN-CO_2 adduct at 160.3 ppm (Fig. 7b), is tentatively assigned to the C atom of CO_2 in DBN-CO_2 adduct [51]. Similarly, the other peak at 163.2 ppm can be attributed to the C atom of CO_2 in $[Tz\text{-}CO_2]^-$ adduct formed by Tz^- reacted with CO_2 [13,52].

FT-IR analyses also provide a consistent profile regarding CO_2 absorption mechanism. As shown in Fig. 8b, no obvious peaks at 3000-3400 cm^{-1} for [2DBN:Tz] before and after CO_2 treatment are observed, indicating that $DBNH^+$ does not react with CO_2 [52]. The peak at 1647 cm^{-1} in fresh [2DBN:Tz] should be assigned to the C=N stretching vibration in DBN, and then it is shielded by a peak at 1668 cm^{-1} which is assigned to the asymmetric stretch of (-N-COO) in both DBN-CO_2 and Tz-CO_2^- adducts after CO_2 treatment [53,54]. The formation of (-N-COO) group is also supported by the appearance of new peaks at 1568 and 1304 cm^{-1} associated with asymmetric and symmetric stretching frequencies of carboxylate $-COO^-$, respectively [52,55]. In addition, a new peak appeared at 813 cm^{-1} can be assigned to the bending mode of carboxylate $-COO^-$ [56].

Postprint. Jiawei Ruan et al. Fuel, Volume 334 (2023) 126709
https://doi.org/10.1016/j.fuel.2022.126709

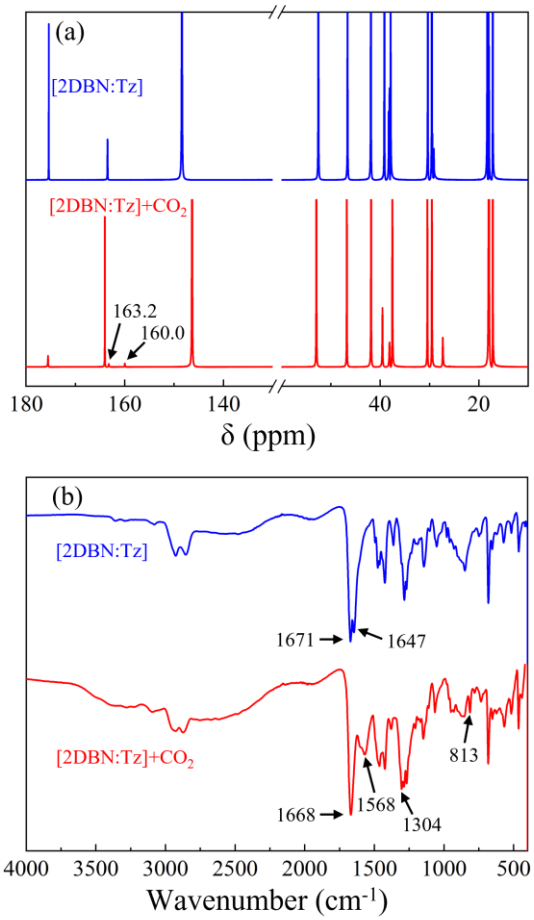

Fig. 8. (a) ^{13}C spectra and (b) FT-IR spectra of [2DBN:Tz] before (blue lines) and after (red lines) CO_2 treatment.

Based on the experimental results, quantum chemistry calculations, ^{13}C NMR, and FT-IR spectra, the plausible absorption mechanism is proposed as presented in Scheme 1. Both molecular DBN and ionic Tz^- in DESs can synergistically interact with CO_2 to produce DBN-CO_2 and Tz-CO_2^- adducts, which is illustrated as Path 1 and Path 2, respectively.

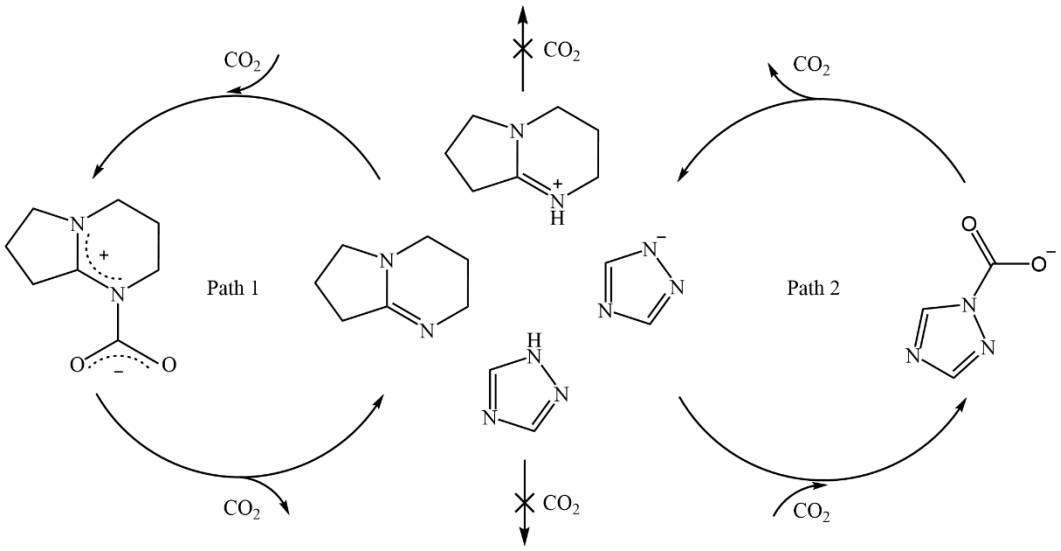

Scheme 1. Plausible synergistic absorption mechanism by DBN molecule (Path 1) and Tz^- ion (Path 2) in DBN-Tz DESs.

Above discussions demonstrate a two-paths CO_2 capture process coordinated by DBN molecule and Tz^- ion which can be tuned by adjusting initial HBA/HBD molar ratio. The DFT calculation of two paths could offer a better understanding of DESs in CO_2 capture.

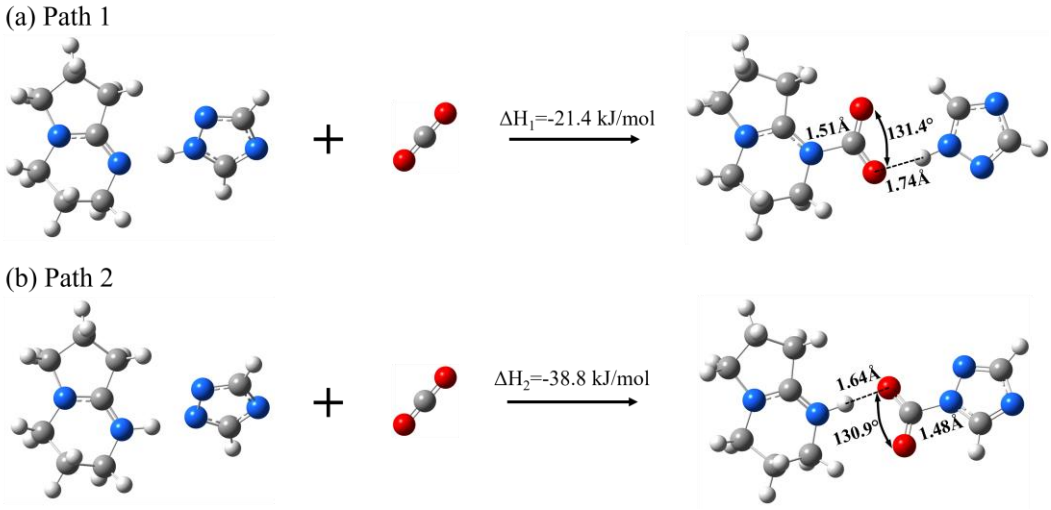

Fig. 9. Possible existing dimer before and after CO_2 absorption along with corresponding enthalpy changes in two paths.

The enthalpy changes of CO_2 absorption by DBN molecule (Path 1) and Tz^- ion (Path 2) together with possible existing dimer after absorption are illustrated in Fig. 9. In Path 1, the formed DBN-CO_2 adduct tends to be stabilized by Tz molecule through hydrogen bond interaction. Similarly, the Tz-CO_2^- adduct formed by Tz^- and CO_2 is stabilized by $DBNH^+$ in Path 2. The O=C-O bond angle of absorbed CO_2 in Path 1 and

Path 2 is 131.4° and 130.9°, respectively, demonstrating the formation of DBN-CO_2 and Tz-CO_2^- adducts. The electron density of BCPs in mol-pair and ion-pair after capturing CO_2 are calculated and shown in Fig. S6 together with mol-pair and ion-pair before CO_2 treatment. The decreasing electron density indicates the reduced interaction strength in DESs after binding with CO_2. Thus, the eutectic nature of DESs may change after CO_2 absorption due to the formation of DBN-CO_2 and Tz-CO_2^- adduct. In addition, the enthalpy change of CO_2 absorption in Path 2 is -38.8 kJ/mol which is lower than that in Path 1, indicating a higher desorption energy consumption of Path 2.

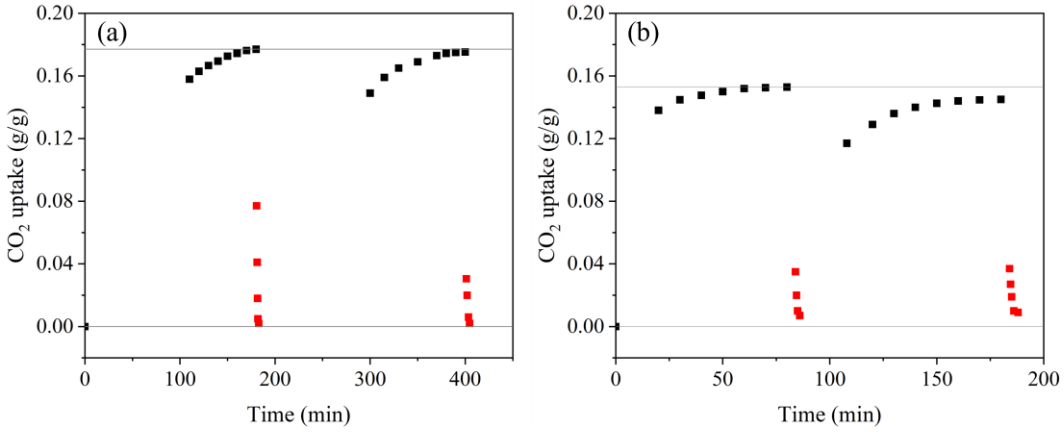

Fig. 10. Absorption and desorption of CO_2 by (a) DBN and (b) [DBN:Tz].

Apart from that, the absorption and desorption performances of DBN and DES [DBN:Tz] are determined and shown in Fig. 10. [DBN:Tz] is selected to represent the CO_2 absorption by Tz^- in Path 2, because the DES composed entirely of Tz^- without DBN molecule is hardly available. By contrast, DBN possesses higher weight capacity than [DBN:Tz], and the corresponding desorption is only 2.5 min at 80 °C, which is shorter than 6 min of [DBN:Tz]. The rapid desorption kinetics of DBN can be attributed to its lower desorption enthalpy change with lower desorption energy consumption. Moreover, the reusability of DBN is better than [DBN:Tz] and the absorption capacity of DBN shows no obvious decrease after recycling.

The fact is that CO_2 absorption in both Path 1 and 2 are exothermic and reversible, resulting in the contrary effect of temperature on absorption rate constants and absorption equilibrium constants. Compared with CO_2 absorption by Tz^-, when DBN absorbs CO_2 at the temperature of 25 °C, the effect of temperature on the reduction of absorption equilibrium constants is more significant than the increase of absorption rate constants. Thus, the equilibration time of CO_2 capture by DBN (180 min) at 25 °C is longer than [DBN:Tz] (60 min) including the contribution of both DBN and Tz^-. Furthermore, the DES [2DBN:Tz] obtains the highest gravimetric capacity approaching 0.19 g CO_2/g DES in 60 min (Fig. 5), also indicating a cooperative and complementary

effect of these two pathways. In short, the synergistic CO_2 absorption mechanism by molecules and ions is also embodied in the absorption and desorption performance of the DESs.

4. Conclusion

DBN and Tz formed DESs were designed and synthesized to absorb CO_2 by synergistic effects of DBN molecule and Tz^- ion in the DESs. The strong hydrogen bond interaction in DBN-Tz DESs was confirmed and exhibited significant melting point depression in DESs. The proton transfer from Tz to DBN was testified and led to form mol-pair and ion-pair in DESs. The absorption capacity of DESs showed a positive correlation with the amount of DBN and ionicity of the DESs, indicating DBN molecule can facilitate CO_2 absorption. Moreover, DBN molecules and Tz^- ions acted as electron-rich nucleophiles can form DBN-CO_2 and Tz-CO_2^- adducts with electrophilic CO_2 through electron transfer. A synergistic CO_2 capture process by DBN and Tz^- in the DESs was illustrated by absorption and desorption performance, demonstrating a complementary effect of these two paths in DESs. The insights into molecules and ions of the DESs and their independent interactions with CO_2 offer a better understanding of these solvents to improve the rational design of DESs for CO_2 capture.

Acknowledgment

The financial support from National Natural Science Foundation of China (22278134) is greatly acknowledged.

References

[1] Bui M, Adjiman CS, Bardow A, Anthony EJ, Boston A, Brown S, et al. Carbon capture and storage (CCS): the way forward. Energy Environ Sci 2018;11(5):1062-176. https://doi.org/10.1039/c7ee02342a.

[2] Chen Y, Liu C, Guo S, Mu T, Wei L, Lu Y. CO_2 capture and conversion to value-added products promoted by MXene-based materials. Green Energy Environ 2022;7(3):394-410. https://doi.org/10.1016/j.gee.2020.11.008.

[3] Chen Y, Mu T. Conversion of CO_2 to value-added products mediated by ionic liquids. Green Chem 2019;21(10):2544-74. https://doi.org/10.1039/c9gc00827f.

[4] Gu Y, Hou Y, Ren S, Sun Y, Wu W. Hydrophobic functional deep eutectic solvents used for efficient and reversible capture of CO_2. ACS Omega 2020;5(12):6809-16. https://doi.org/10.1021/acsomega.0c00150.

[5] Seo S, Quiroz-Guzman M, DeSilva MA, Lee TB, Huang Y, Goodrich BF, et al. Chemically tunable ionic liquids with aprotic heterocyclic anion (AHA) for CO_2 capture. J Phys Chem B 2014;118(21):5740-51. https://doi.org/10.1021/jp502279w.

[6] Chen Y, Liu C, Duan Y, Yu D, Liu Z, Li Y, et al. Room-temperature conversion of CO_2 into quinazoline-2,4(1H,3H)-dione by deep eutectic solvents at atmospheric pressure with high efficiency. React Chem Eng 2022;7:1968-77. https://doi.org/10.1039/D2RE00137C.

[7] Bernhardsen IM, Knuutila HK. Kinetics of CO_2 absorption into aqueous solutions of 3-dimethylamino-1-propanol and 1-(2-hydroxyethyl)pyrrolidine in the blend with 3-(methylamino)propylamine. Chem Eng Sci: X 2019;3:100032. https://doi.org/10.1016/j.cesx.2019.100032.

[8] Nittaya T, Douglas PL, Croiset E, Ricardez-Sandoval LA. Dynamic modelling and control of MEA absorption processes for CO_2 capture from power plants. Fuel 2014;116:672-91. https://doi.org/10.1016/j.fuel.2013.08.031.

[9] Khalifa O, Alkhatib III, Bahamon D, Alhajaj A, Abu-Zahra MRM, Vega LF. Modifying absorption process configurations to improve their performance for post-combustion CO_2 capture - what have we learned and what is still missing? Chem Eng J 2022;430:133096. https://doi.org/10.1016/j.cej.2021.133096.

[10] Wang J, Song Z, Cheng H, Chen L, Deng L, Qi Z. Computer-aided design of ionic liquids as absorbent for gas separation exemplified by CO_2 capture cases. ACS Sustain Chem Eng 2018;6(9):12025-35. https://doi.org/10.1021/acssuschemeng.8b02321.

[11] Chen L, Xiong Y, Qin H, Qi Z. Advances of ionic liquids and deep eutectic solvents in green processes of biomass-derived 5-hydroxymethylfurfural. ChemSusChem 2022;15(13):e202102635. https://doi.org/10.1002/cssc.202102635.

[12] Bates ED, Mayton RD, Ntai I, Davis JH. CO_2 capture by a task-specific ionic liquid. J Am Chem Soc 2002;124(6):926-7. https://doi.org/10.1021/ja017593d.

[13] Wang C, Luo X, Luo H, Jiang D, Li H, Dai S. Tuning the basicity of ionic liquids for equimolar CO_2 capture. Angew Chem Int Ed 2011;50(21):4918-22. https://doi.org/10.1002/anie.201008151.

[14] Taylor SFR, McCrellis C, McStay C, Jacquemin J, Hardacre C, Mercy M, et al. CO_2 capture in wet and dry superbase ionic liquids. J Solution Chem 2015;44(3-4):511-27. https://doi.org/10.1007/s10953-015-0319-z.

[15] Li F, Bai Y, Zeng S, Liang X, Wang H, Huo F, et al. Protic ionic liquids with low viscosity for efficient and reversible capture of carbon dioxide. Int J Greenh Gas Control 2019;90:102801. https://doi.org/10.1016/j.ijggc.2019.102801.

[16] Jessop PG, Heldebrant DJ, Li X, Eckert CA, Liotta CL. Reversible nonpolar-to-polar solvent.

Nature 2005;436(7054):1102. https://doi.org/10.1038/4361102a.

[17] Bhattacharyya S, Filippov A, Shah FU. High CO_2 absorption capacity by chemisorption at cations and anions in choline-based ionic liquids. Phys Chem Chem Phys 2017;19(46):31216-26. https://doi.org/10.1039/c7cp07059d.

[18] Huang Z, Jiang B, Yang H, Wang B, Zhang N, Dou H, et al. Investigation of glycerol-derived binary and ternary systems in CO_2 capture process. Fuel 2017;210:836-43. https://doi.org/10.1016/j.fuel.2017.08.043.

[19] Zhang N, Huang Z, Zhang H, Ma J, Jiang B, Zhang L. Highly efficient and reversible CO_2 capture by task-specific deep eutectic solvents. Ind Eng Chem Res 2019;58(29):13321-9. https://doi.org/10.1021/acs.iecr.9b02041.

[20] Suo X, Yang Z, Fu Y, Do-Thanh CL, Chen H, Luo H, et al. CO_2 chemisorption behavior of coordination-derived phenolate sorbents. ChemSusChem 2021;14(14):2854-9. https://doi.org/10.1002/cssc.202100666.

[21] Nordness O, Brennecke JF. Ion dissociation in ionic liquids and ionic liquid solutions. Chem Rev 2020;120(23):12873-902. https://doi.org/10.1021/acs.chemrev.0c00373.

[22] Smith EL, Abbott AP, Ryder KS. Deep eutectic solvents (DESs) and their applications. Chem Rev 2014;114(21):11060-82. https://doi.org/10.1021/cr300162p.

[23] Stoimenovski J, Izgorodina EI, MacFarlane DR. Ionicity and proton transfer in protic ionic liquids. Phys Chem Chem Phys 2010;12(35):10341-7. https://doi.org/10.1039/c0cp00239a.

[24] Sun X, Liu S, Khan A, Zhao C, Yan C, Mu T. Ionicity of acetate-based protic ionic liquids: Evidence for both liquid and gaseous phases. New J Chem 2014;38(8):3449-56. https://doi.org/10.1039/c4nj00384e.

[25] Nasrabadi AT, Gelb LD. How proton transfer equilibria influence ionic liquid properties: Molecular simulations of alkylammonium acetates. J Phys Chem B 2018;122(22):5961-71. https://doi.org/10.1021/acs.jpcb.8b01631.

[26] Shen M, Zhang Y, Chen K, Che S, Yao J, Li H. Ionicity of protic ionic liquid: Quantitative measurement by spectroscopic methods. J Phys Chem B 2017;121(6):1372-6. https://doi.org/10.1021/acs.jpcb.6b11624.

[27] Fu H, Hou Y, Sang H, Mu T, Lin X, Peng Z, et al. Carbon dioxide capture by new DBU-based DES: The relationship between ionicity and absorptive capacity. AlChE J 2021;67(7):e17244. https://doi.org/10.1002/aic.17244.

[28] Hu X, Wang J, Mei M, Song Z, Cheng H, Chen L, et al. Transformation of CO_2 incorporated in adducts of N-heterocyclic carbene into dialkyl carbonates under ambient conditions: An experimental and mechanistic study. Chem Eng J 2021;413:127469. https://doi.org/10.1016/j.cej.2020.127469.

[29] Wang J, Cheng H, Song Z, Chen L, Deng L, Qi Z. Carbon dioxide solubility in phosphonium-based deep eutectic solvents: An experimental and molecular dynamics study. Ind Eng Chem Res 2019;58(37):17514-23. https://doi.org/10.1021/acs.iecr.9b03740.

[30] Mei M, Hu X, Song Z, Chen L, Deng L, Qi Z. CO_2 capture by 1-ethyl-3-methylimidazolium acetate: Solubility at low pressure and quantification of chemisorption and physisorption. J Mol Liq 2022;348:118036. https://doi.org/10.1016/j.molliq.2021.118036.

[31] Marenich AV, Cramer CJ, Truhlar DG. Universal solvation model based on solute electron density and on a continuum model of the solvent defined by the bulk dielectric constant and atomic surface tensions. J Phys Chem B 2009;113(18):6378-96. https://doi.org/10.1021/jp810292n.

[32] Talebian E, Talebian M. A general review on the derivation of Clausius–Mossotti relation. Optik 2013;124(16):2324-6. https://doi.org/10.1016/j.ijleo.2012.06.090.

[33] Lu T, Chen F. Multiwfn: A multifunctional wavefunction analyzer. J Comput Chem 2012;33(5):580-92. https://doi.org/10.1002/jcc.22885.

[34] Song Z, Hu X, Wu H, Mei M, Linke S, Zhou T, et al. Systematic screening of deep eutectic solvents as sustainable separation media exemplified by the CO_2 capture process. ACS Sustain Chem Eng 2020;8(23):8741-51. https://doi.org/10.1021/acssuschemeng.0c02490.

[35] Guo W, Hou Y, Ren S, Tian S, Wu W. Formation of deep eutectic solvents by phenols and choline chloride and their physical properties. J Chem Eng Data 2013;58(4):866-72. https://doi.org/10.1021/je300997v.

[36] Wang R, Qin H, Song Z, Cheng H, Chen L, Qi Z. Toward reactive extraction processes for synthesizing long-chain esters: A general approach by tuning bifunctional deep eutectic solvent. Chem Eng J 2022;445:136664. https://doi.org/10.1016/j.cej.2022.136664.

[37] Lu T, Chen Q. Independent gradient model based on Hirshfeld partition: A new method for visual study of interactions in chemical systems. J Comput Chem 2022;43(8):539-55. https://doi.org/10.1002/jcc.26812.

[38] Chen K, Wang Y, Yao J, Li H. Equilibrium in protic ionic liquids: The degree of proton transfer and thermodynamic properties. J Phys Chem B 2018;122(1):309-15. https://doi.org/10.1021/acs.jpcb.7b10671.

[39] Golubev NS, Denisov GS, Smirnov SN, Shchepkin DN, Limbach HH. Evidence by NMR of temperature-dependent solvent electric field effects on proton transfer and hydrogen bond geometries. 1996;196(1):73-84.

[40] Sun X, Cao B, Zhou X, Liu S, Zhu X, Fu H. Theoretical and experimental studies on proton transfer in acetate-based protic ionic liquids. J Mol Liq 2016;221:254-61. https://doi.org/10.1016/j.molliq.2016.05.080.

[41] Rozas I, Alkorta I, Elguero J. Behavior of ylides containing N, O, and C atoms as hydrogen bond acceptors. J Am Chem Soc 2000;122(45):11154-61. https://doi.org/10.1021/ja0017864.

[42] Yang M, Huang D, Wu H, Zhang H, An P, Yuan C, et al. Unravelling the weak interactions in binary clusters of serotonin and amino acid residues. ChemistrySelect 2019;4(34):9978-86. https://doi.org/10.1002/slct.201902100.

[43] Pérez ER, Santos RHA, Gambardella MTP, de Macedo LGM, Rodrigues-Filho UP, Launay J-C, et al. Activation of carbon dioxide by bicyclic amidines. J Org Chem 2004;69(23):8005-11. https://doi.org/10.1021/jo049243q.

[44] Taylor SFR, McClung M, McReynolds C, Daly H, Greer AJ, Jacquemin J, et al. Understanding the competitive gas absorption of CO_2 and SO_2 in superbase ionic liquids. Ind Eng Chem Res 2018;57(50):17033-42. https://doi.org/10.1021/acs.iecr.8b03623.

[45] Cao J, Ren Q, Chen F, Lu T. Comparative study on the methods for predicting the reactive site of nucleophilic reaction. Science China Chemistry 2015;58(12):1845-52. https://doi.org/10.1007/s11426-015-5494-7.

[46] Singh P, Niederer JPM, Versteeg GF. Structure and activity relationships for amine-based CO_2 absorbents-II. Chem Eng Res Des 2009;87(2):135-44. https://doi.org/10.1016/j.cherd.2008.07.014.

[47] Doran JL, Hon B, Leopold KR. Rotational spectrum and structure of the pyridine-CO_2 van der Waals complex. J Mol Struct 2012;1019:191-5. https://doi.org/10.1016/j.molstruc.2012.03.039.

[48] Pereira FS, Lincon da Silva Agostini D, do Espírito Santo RD, deAzevedo ER, Bonagamba TJ, Job AE, et al. A comparative solid state ^{13}C NMR and thermal study of CO_2 capture by amidines PMDBD and DBN. Green Chem 2011;13(8):2146-53. https://doi.org/10.1039/c1gc15457e.

[49] Buckingham AD, Pople JA. High-resolution NMR spectra in electric fields. 1963;59:2421-30.

[50] Villiers C, Dognon JP, Pollet R, Thuery P, Ephritikhine M. An isolated CO_2 adduct of a nitrogen base: Crystal and electronic structures. Angew Chem Int Ed 2010;49(20):3465-8. https://doi.org/10.1002/anie.201001035.

[51] Pérez ER, da Silva MO, Costa VC, Rodrigues-Filho UP, Franco DW. Efficient and clean synthesis of N-alkyl carbamates by transcarboxylation and O-alkylation coupled reactions using a DBU-CO_2 zwitterionic carbamic complex in aprotic polar media. Tetrahedron Lett 2002;43(22):4091-3. https://doi.org/10.1016/S0040-4039(02)00697-4.

[52] Xu Y. CO_2 absorption behavior of azole-based protic ionic liquids: Influence of the alkalinity and physicochemical properties. J CO_2 Util 2017;19:1-8. https://doi.org/10.1016/j.jcou.2017.03.001.

[53] Luo X, Guo Y, Ding F, Zhao H, Cui G, Li H, et al. Significant improvements in CO_2 capture by pyridine-containing anion-functionalized ionic liquids through multiple-site cooperative interactions. Angew Chem Int Ed 2014;53(27):7053-7. https://doi.org/10.1002/anie.201400957.

[54] Hu X, Yang X, Chen L, Mei M, Song Z, Fei Z, et al. Elucidating the transition between CO_2 physisorption and chemisorption in 1,2,4-triazolate ionic liquids at a molecular level. Chem Eng J 2022;435:134956. https://doi.org/10.1016/j.cej.2022.134956.

[55] Zhang K, Hou Y, Wang Y, Wang K, Ren S, Wu W. Efficient and reversible absorption of CO_2 by functional deep eutectic solvents. Energy Fuels 2018;32(7):7727-33. https://doi.org/10.1021/acs.energyfuels.8b01129.

[56] Trivedi TJ, Lee JH, Lee HJ, Jeong YK, Choi JW. Deep eutectic solvents as attractive media for CO_2 capture. Green Chem 2016;18(9):2834-42. https://doi.org/10.1039/c5gc02319j.